Molecular Catalysis 443 (2017) 69–77

Contents lists available at ScienceDirect

Molecular Catalysis

journal homepage: www.elsevier.com/locate/mcat

MCAT

Nanosheet-enhanced efficiency in amine-catalyzed asymmetric epoxidation of α, β-unsaturated aldehydes via host-guest synergy

Hui Liu, Zhe An, Jing He*

State Key Laboratory of Chemical Resource Engineering, Beijing University of Chemical Technology, Beijing 100029, China

ARTICLE INFO

Article history:
Received 19 April 2017
Received in revised form
14 September 2017
Accepted 30 September 2017

Keywords:
LDH nanosheet
Asymmetric epoxidation
Organocatalysis
Solid bases
Rigid substituent

ABSTRACT

Amine-catalyzed asymmetric epoxidation of α, β-unsaturated aldehydes has been promoted by attaching the nanosheets of layered double hydroxides (LDHs), a natural and/or synthetic anionic layered compound. 76% of epoxide yield and 93% ee of major diastereomer have been afforded in the asymmetric epoxidation of cinnamaldehyde. The amine sites employed here are the amino group in α-amino acid anion intercalated in the interlayer space of LDHs. The nanosheets of LDHs have been revealed to play key role in the enhancement of catalytic activity by affording the desired basicity and the boost of enantioselectivity by serving as the rigid substituent of amino acids. The hydrophobic interlayer microenvironment and ordered arrangement of intercalated amino acid anions additionally contribute to the catalytic efficacy. Stronger interlayer hydrophobicity favors the conversion and epoxide yield and better arrangement of interlayer anions favors the ee.

1. Introduction

Catalytic enantioselective epoxidation of olefins holds a prominent place in organic chemistry [1–3] since the optically active epoxy products are both valuable organic intermediate [4,5] and important building blocks in pharmaceuticals [6–8]. For example, epoxy products ethyl (2R, 3*R*)-3-phenylglycidate can be used for the synthesis of side chain of Taxol, a frontline anticancer drug for the treatment of ovarian, breast, and lung cancer [9–11]. For enantiopure epoxide preparation, the kinetic resolution of racemic epoxides was initially employed [12–16]. Lately, in terms of overall cost, reaction speed, raw material availability, and robustness, asymmetric catalytic epoxidation was developed. The pioneer work of enantioselective epoxidation of olefins was achieved on organometallic catalysts [17–19]. Katsuki and Sharpless demonstrated that the titanium-tartrate complexes were highly efficient asymmetric epoxidation catalysts of allylic alcohols [20]. Chiral manganese-salen complexes were reported as excellent catalysts for the asymmetric epoxidation of conjugated *cis*-disubstituted olefins [21]. The complexes of Li [22], Mg [23,24], Sc [25], Zn [26–31], Fe [32–41], and lanthanides [42–48] have been employed for the asymmetric epoxidation of α, β-unsaturated ketones, esters, and amides. Recently, small organic molecules have been used as the asymmetric epoxidation catalysts because of their notable advantages over metal complexes, such as lower cost, better resistance to moisture and oxygen, and absence of metal residues and toxicity in products [49–52]. The organocatalysts employed for the enantioselective epoxidation of olefins include phase-transfer catalysts [53–56], peptide-type catalysts [57,58], chiral ketone catalysts [52,59], and chiral amine catalysts [60–63].

Enantiomerically enriched α, β-epoxy carbonyl compounds (such as α, β-epoxy aldehyde [4,5,64], α, β-epoxy ketone [7], and α, β-epoxy ester [65]) are especially useful in total synthesis. Chiral amine catalysts were found to be very efficient organocatalysts in the asymmetric epoxidation of α, β-unsaturated carbonyl compounds via iminium-activation mechanism and steric-shielding approach. Following the iminium-activation of carbonyl by amine sites, the carbon–carbon double bonds in the resulting iminium intermediate are inclined to be nucleophilic attacked by activated oxidant. In order to facilitate the activation of oxidant, exogenous additives, such as NaOH, KOH, Urea, Na_2CO_3, $NaHCO_3$ [66–69] trifluoroacetic acid, achiral or chiral phosphoric acids [61–63], were generally used. The use of solid bases, which are much more environment-friendly and green, to assist the activation of oxidant has not been reported so far in the enantioselective epoxidation of olefins. The attack of activated oxidant to the iminium intermediate is the enantioselectivity determining step. Computational [70] and experimental results both revealed that the catalysts with more hindered structures, such as the pyrrolidine-derivatives with

* corresponding author at: Postal address: Box 98, 15 Beisanhuan Dong Lu, Beijing 100029, China.
E-mail address: jinghe@263.net.cn (J. He).

http://dx.doi.org/10.1016/j.mcat.2017.09.035
2468-8231/

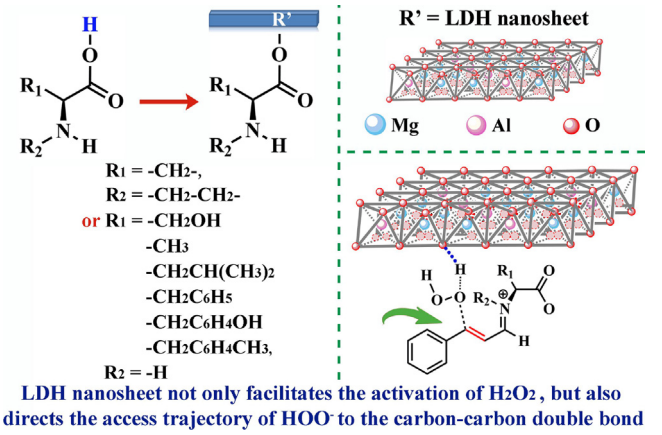

Scheme 1. Schematic illustration of LDH nanosheets as both solid base and rigid planar substituent for α-amino acids.

sterically encumbered aryl [70–72], the peptides with a minimum of one helical turn [58,59,73] afforded better asymmetric induction via steric-shielding approach. Those effective catalysts with bulky and complicated entities usually require complicated multi-step synthesis and are often very expensive. Elaborately designed strategies, which are facile but could effectively afford remarkable enantioselectivity, are highly desired.

Here, we propose an efficient strategy to promote amine-catalyzed asymmetric epoxidation of α, *β*-unsaturated aldehyde, which simply utilizes inorganic nanosheets to supply the desired basicity and steric hindrance around the amine sites (Scheme 1). The inorganic nanosheets employed here are the positively-charged brucite-like layers of layered double hydroxides (LDHs), a natural and/or synthetic anionic compound and also a well-known basic catalyst [74–77]. The strategy proposed here demonstrates efficacy, in that 76% of yield, 82:18 of dr (trans:cis), and 93% of ee for major diastereomer (trans) have been afforded in the asymmetric epoxidation of cinnamaldehyde.

2. Experimental

2.1. General

L-Serine, L-alanine, L-leucine, L-phenylalanine, L-tyrosine, 4-methy-L-phenylalanine, L-proline, α-methyl-L-proline, cinnamaldehyde, 4-methyl-cinnamaldehyde, 4-chloro-cinnamaldehyde, 4-trifluoromethyl- cinnamaldehyde, 30% aqueous H_2O_2, dimethyl maleate, pyrene, and (2*S*)-2-[Bis[3,5-bis(trifluoromethyl)phenyl](trimethylsiloxy)methyl]pyrrolidine (the Jørgensen-Hayashi catalyst) were purchased from Sigma-Aldrich and Alfa-Aesar. All the reagents and commercial chemicals were of analytical purity and used as received without further purification.

The powder X-ray diffraction (XRD) patterns were taken on a Shimadzu XRD-6000 diffractometer with Cu Ka radiation (40 kV and 30 mA) at a scanning rate of 5°/min and step size of 0.02°. The content of Mg, Ni, Zn, Ca, and Al was determined on inductively coupled plasma (ICP) atomic emission spectrophotometry (Shimadzu ICPs-7500) by dissolving the samples in dilute HNO_3. The C, H and N element analysis was performed on an Elementar Co. Vario elemental analyzer. The Fourier transform infrared (FT-IR) spectra were recorded on a Bruker Vector 22 FT-IR spectrometer with a resolution of 4 cm^{-1} using the standard KBr pellet method. The fluorescence spectra were recorded at room temperature on a Shimadzu RF-5301PC spectrophotometer operating in the spectrum mode. ^1H spectra were recorded in $CDCl_3$ solutions on Bruker Avance 400 MHz NMR spectrometer (Bruker, Bremen, Germany) at ambient temperature. ^1H NMR data are reported as the following: chemical shift in parts per million (δ, ppm) from chloroform ($CHCl_3$) taken as 7.26 ppm, intergration, multiplicity (s = singlet, d = doublet, t = triplet, q = quartet, m = multiplet, dd = doublet of doublets) and coupling constant (Hz). The reaction progress was monitored by TLC (hexane/ethyl acetate (v/v = 4/1)). All the molecular dynamics simulations were performed using the Discover module in the Materials Studio software package.

2.2. Preparation of α-amine acid anions intercalated LDH nanosheets

The preparation of α-amine acid anions intercalated M^{II}/Al-LDHs (M^{II} = Mg, Ni, Zn, or Ca, α-amine acid (AA) = L-serine, L-alanine, L-leucine, L-phenylalanine, L-tyrosine, or 4-methy-L-phenylalanine) were accomplished through the coprecipitation approach [78,79] by addition of a mixed solution of 1 M $M(NO_3)_2$ (M = Mg, Ni, Zn, or Ca) and $Al(NO_3)_3$ dropwise to a stirred 50 mM α-amine acid solution, with a molar ratio of M^{2+}/Al^{3+}/α-amine acid anions molar ratio = 2/1/1. The solution pH was maintained at 10 for α-amine acid anions intercalated Mg/Al-LDHs, 8 for α-amine acid anions intercalated Ni/Al-LDHs, 9 for α-amine acid anions intercalated Zn/Al-LDHs, and 11.5 for α-amine acid anions intercalated Ca/Al-LDHs. by dropwise addition of 1 M NaOH solution under stirring. The suspension was stirred at 313 K in N_2 atmosphere for 6 h. The resulting suspension was filtrated, washed thoroughly with decarbonated deionized water and anhydrous alcohol, and dried in a vacuum oven at room temperature. The preparation of Mg/Al-Pro-LDHs and Mg/Al-Me-Pro-LDHs was accomplished through the reconstruction method [80]. The Mg/Al-CO_3^{2-}-LDHs precursor was first synthesized by addition of a mixed solution of 0.16 M $Mg(NO_3)_2$ and $Al(NO_3)_3$ (Mg/Al molar ratio = 2/1) in 225 mL of deionized water to a stirred solution of NaOH and Na_2CO_3 in 225 mL of deionized water with pH maintained at 9.5. The concentration of the base was related to the concentration of metal ions: [NaOH] = 1.6 [$Mg^{2+} + Al^{3+}$] and [CO_3^{2-}] = 2.0 [Al^{3+}]. The suspension was aged at 373 K for 18 h. The final precipitate was filtered, washed thoroughly with deionized water and anhydrous alcohol, and dried at 333 K for 24 h. The Mg/Al-CO_3^{2-}-LDHs was then calcined at 773 K for 5 h with a temperature-programmed rate of 5 K/min from room temperature to 773 K, and then naturally cooled, producing layered double oxides (LDO). 0.5 g of LDO was added to a freshly prepared solution of 0.006 mol (or 0.009 mol) of L-proline or α-methyl-L-proline and 0.006 mol (or 0.009 mol) of NaOH in 100 mL of decarbonated deionized water. The suspension was stirred at 298 K in N_2 atmosphere for 24 h. The resulting precipitate was filtered, washed thoroughly with decarbonated deionized water and anhydrous ethanol, and dried in a vacuum oven at 313 K.

2.3. General procedure for the asymmetric epoxidation reactions and catalyst recycling

Without any particular precautions to extrude oxygen or moisture, 0.25 mmol α, *β*-unsaturated aldehyde and 1.06 equiv. of H_2O_2 (30% aqueous solution) in 1 mL acetone were weighted in a flask and allowed to stir for 10 min M^{II}/Al-AA-LDHs (AA: 10 mol%) was then added and the reaction was sealed and allowed to stir at 25 °C. In 3 or 4 h, the solid catalyst was recovered by filtration, and the reaction mixture was quenched by H_2O, extracted with Et_2O. The water phase was washed for two times with Et_2O. The organic phase was then dried over anhydrous Na_2SO_4 and evaporated to give the epoxy aldehydes.

For easy identification, the epoxy aldehydes were reduced to the corresponding epoxy alcohols by $NaBH_4$. The epoxy aldehydes were redissolved in 1 mL MeOH and cooled to 0 °C, then followed by

addition of $NaBH_4$ (25 mg). After 30 min, the reaction was quenched by saturated NH_4Cl, extracted with Et_2O, dried over anhydrous Na_2SO_4 and concentrated in vacuo. Dimethyl maleate (1 equiv.) was added into the crude product as internal standard. The conversion, yield, and dr were determined by ^1H NMR. The ee were determined by HPLC analysis on chiral OD-H or OJ-H column for aromatic compounds or by Mosher's MTPA method for aliphatic compounds.

After the reaction terminated, the solid catalyst was recovered by filtration and washed with 5 mL Et_2O for three times. Then the solid was dried in a vacuum oven at 313 K and used directly for the next catalytic reaction.

2.4. Detection of interlayer hydrophobicity

To determine the interlayer hydrophobic microenvironment, pyrene was used as a fluorescent probe [81]. Batch sorption experiments were performed in 50-mL centrifuge tubes with Teflon-lined screw caps. For each experiment, the Mg/Al-AA-LDHs with the same amount of α-amine acid anions were dried under a flow of dry N_2 to remove any surface-bound solvent. Then 30 mL of the corresponding liquid phases ($v_{water}/v_{methanol}$ = 1/1) was added to the tubes. Pyrene was added to the tubes by direct injection of an aqueous solution of pyrene and kept constant at 1 μM. The centrifuge tubes were sealed and wrapped with aluminum foil to protect them from light and placed on a wrist shaker for 24 h. The tubes were removed from the shaker, placed horizontally on a bench, and shaken for the following 2 days. Then the pyrene-loaded Mg/Al-amine acid anions-LDHs were obtained by centrifugation. The solid was dried under a flow of dry N_2 and analyzed with a Shimadzu RF-5301PC spectrometer. Samples were excited at λ = 335 nm and pyrene emission spectra were recorded from 350 to 490 nm. Both excitation and emission slit widths were set at 2.5 nm.

2.5. Structural model and molecular dynamics (MD) simulation method

MD simulations were used to understand the arrangement of α-amine acid anions in the Mg/Al-LDHs interlayer space. The lattice containing 18 Mg atoms and 9 Al atoms was built on the basis of each [AlO_6] octahedron surrounded by six [MgO_6] and each [MgO_6] octahedron, in turn, surrounded by three [AlO_6] octahedron, because the ratio of Mg to Al is 2:1, which ensures that Al atoms will not occupy adjacent octahedron. According to the literature [82,83], the lattice parameters of the 2-dimensional layer are $a = b = 3.142$ Å. On the basis of the model of the host layer, a supercell was constructed, with lattice parameter $a = 28.278$ Å, $b = 9.426$ Å, and the initial interlayer spacing 17.960 Å for $Mg_{2.03}$/Al-$Phe_{0.79}$-LDHs and 18.170 Å for $Mg_{2.03}$/Al-Me-$Phe_{0.97}$-LDHs, $\alpha = \beta = 90^\circ$, $\gamma = 120^\circ$ (equivalent to $9 \times 3 \times 1$ in the *a*, *b*, and *c* directions). The supercell was treated as *P*1 symmetry and all of lattice parameters were considered as independent variables during the simulation. A 3-dimensional periodic boundary condition was applied to the system, so the simulated supercell can be repeated infinitely in three directions. Then, for maintaining the whole system electrically neutral and matching the chemical compositions, seven L-phenylalanine anions, one carbonate ion, and twenty eight water molecules were introduced into the simulated supercell randomly for $Mg_{2.03}$/Al-$Phe_{0.79}$-LDHs and eight 4-methy-L-phenylalanine anions, one nitrate ion, and thirty six water molecules were introduced for $Mg_{2.03}$/Al-Me-$Phe_{0.97}$-LDHs. All MD simulations were performed by adopting the LDHFF force field developed by Zhang et al. [84]. After energy minimization was applied on the initial models, MD simulations were performed in an isothermal–isobaric (NPT) ensemble with the temperature of 298 K and the pressure of 0.1 MPa (about 1 atm). Temperature and pressure control were performed using the Andersen method [85] and the Berendsen method [86], respectively. Long-range Coulombic interactions and van der Waals interactions were computed by the Ewald summation technique. The simulation time-step was set to be 1 fs and the total simulation time was 200 ps. All the simulations were performed using the Discover module in the Material Studio software package [87].

3. Results and discussion

3.1. Structural properties of α-amine acid anions intercalated LDH nanosheets

The nanosheets employed here are the brucite-like layers of magnesium and aluminum hydroxides (Mg/Al-LDHs), calcium and aluminum hydroxides (Ca/Al-LDHs), nickel and aluminum hydroxides (Ni/Al-LDHs), and zinc and aluminum hydroxides (Zn/Al-LDHs). The amine sites employed here are the amino group in alpha-amino acid anion intercalated in the interlayer space of LDHs. The intercalation of L-serine (Ser), L-alanine (Ala), L-leucine (Leu), L-phenylalanine (Phe), L-tyrosine (Tyr), and 4-methy-L-phenylalanine (Me-Phe) was performed by the co-precipitation method and of L-proline (Pro) and α-methyl-L-proline (Me-Pro) by the reconstruction method. The basal spacing is calculated from the 003 reflection of the XRD patterns (Fig. 1, A) as 0.90, 0.88, 0.88, 1.80, 1.50, 1.82, 0.78, 0.78, 1.75, 1.65, and 1.82 nm for Mg/Al-Ser-LDHs, Mg/Al-Ala-LDHs, Mg/Al-Leu-LDHs, Mg/Al-Phe-LDHs, Mg/Al-Tyr-LDHs, Mg/Al-Me-Phe-LDHs, Mg/Al-Pro-LDHs, Mg/Al-Me-Pro-LDHs, Ca/Al-Phe-LDHs, Ni/Al-Phe-LDHs, and Zn/Al-Phe-LDHs. Subtracting the brucite-like layer thickness (0.48 nm) from the calculated basal spacing, the interlayer spacing is estimated to be 0.42, 0.40, 0.40, 1.32, 1.02, 1.34, 0.30, 0.30, 1.27, 1.17, and 1.34 nm, indicating a monolayer tilted arrangement of interlayer amino acid anions for Mg/Al-Ser-LDHs, Mg/Al-Ala-LDHs, or Mg/Al-Leu-LDHs, monolayer horizontal arrangement for Mg/Al-Pro-LDHs or Mg/Al-Me-Pro-LDHs, bilayer vertical arrangement for Mg/Al-Phe-LDHs, Mg/Al-Tyr-LDHs, Mg/Al-Me-Phe-LDHs, Ca/Al-Phe-LDHs, Ni/Al-Phe-LDHs, or Zn/Al-Phe-LDHs (Fig. 1, B) in light of the dimension of α-amino acid anions measured by Materials Studio Program (Fig. S1). It is interesting that the aliphatic α-amino acid anions are all arranged in monolayer and the aromatic α-amino acid anions in bilayer in the interlayer regions. The M^{2+}/Al^{3+} molar ratio was determined according to the ICP results as in a narrow range of 1.78–2.22 for the LDHs intercalated with primary α-amino acid anions, and 2.70 for the LDHs intercalated with L-proline or α-methyl-L-proline anions (Table S1). The interlayer α-amino acid anions were determined according to the CHN results in the percentage of 21% to 33% for the case of monolayer arrangement, and 64% to 97% for the case of bilayer arrangement (Table S1). The rest of interlayer anions are co-existing carbonate and/or nitrate. The asymmetric (υ_{COOas}) and symmetric vibrations (υ_{COOs}) of carboxylate group in the LDH nanosheets-attached α-amine acid anions are resolved at 1607 and 1348 cm^{-1} for $Mg_{2.03}$/Al-$Ser_{0.21}$-LDHs, 1617 and 1357 cm^{-1} for $Mg_{2.03}$/Al-$Ala_{0.21}$-LDHs, 1580 and 1362 cm^{-1} for $Mg_{1.78}$/Al-$Leu_{0.22}$-LDHs, 1591 and 1354 cm^{-1} for $Mg_{2.03}$/Al-$Phe_{0.79}$-LDHs, 1597 and 1362 cm^{-1} for $Mg_{2.22}$/Al-$Tyr_{0.71}$-LDHs, 1593 and 1363 cm^{-1} for $Mg_{2.03}$/Al-Me-$Phe_{0.97}$-LDHs, 1577 and 1369 cm^{-1} for $Mg_{2.70}$/Al-$Pro_{0.26}$-LDHs, 1581 and 1389 cm^{-1} for $Mg_{2.70}$/Al-$Pro_{0.33}$-LDHs, 1574 and 1361 cm^{-1} for $Mg_{2.70}$/Al-$Pro_{0.33}$-LDHs, 1573 and 1354 cm^{-1} for $Ca_{2.03}$/Al-$Phe_{0.64}$-LDHs, 1579 and 1362 cm^{-1} for $Ni_{1.78}$/Al-$Phe_{0.97}$-LDHs, and 1577 and 1360 cm^{-1} for $Zn_{1.86}$/Al-$Phe_{0.66}$-LDHs in the FT-IR spectra (Fig. 1, C). The $\Delta\upsilon_{COO}$ ($\upsilon_{COOas} - \upsilon_{COOs}$) is 259, 260, 218, 237, 235, 230, 208, 192, 213, 219, 217, and 217 cm^{-1}, respectively. The $\Delta\upsilon_{COO}$ of the corresponding α-amine acid sodium salt [88–95] is 207,

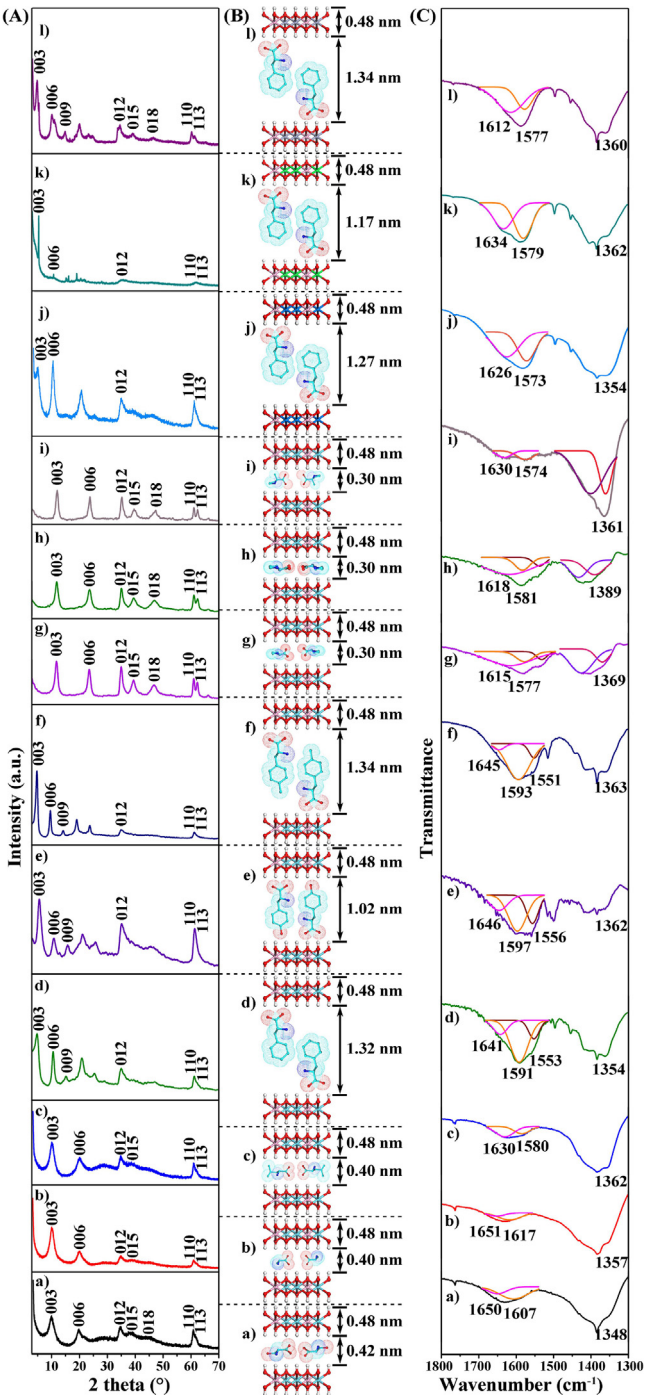

Fig. 1. The XRD patterns (A), schematic structures (B), and FT-IR spectra (C) of a) $Mg_{2.03}$/Al-$Ser_{0.21}$-LDHs, b) $Mg_{2.03}$/Al-$Ala_{0.21}$-LDHs, c) $Mg_{1.78}$/Al-$Leu_{0.22}$-LDHs, d) $Mg_{2.03}$/Al-$Phe_{0.79}$-LDHs, e) $Mg_{2.22}$/Al-$Tyr_{0.71}$-LDHs, f) $Mg_{2.03}$/Al-Me-$Phe_{0.97}$-LDHs, g) $Mg_{2.70}$/Al-$Pro_{0.26}$-LDHs, h) $Mg_{2.70}$/Al-$Pro_{0.33}$-LDHs, i) $Mg_{2.70}$/Al-Me-$Pro_{0.26}$-LDHs, j) $Ca_{2.03}$/Al-$Phe_{0.64}$-LDHs, k) $Ni_{1.78}$/Al-$Phe_{0.97}$-LDHs, and l) $Zn_{1.86}$/Al-$Phe_{0.66}$-LDHs.

213, 175, 216, 193, 212, 196, 196, 181, 216, and 216 cm^{-1}. Following the method reported in literature [96,97] by comparing the $\Delta\upsilon_{COO}$ between the value of the interlayer α-amino acid anions with the value of the corresponding α-amino acid sodium salts, the electrostatic interactions between the brucite-like layer and α-amino acid anions were identified as monodentate mode for $Mg_{2.03}$/Al-$Ser_{0.21}$-LDHs, $Mg_{2.03}$/Al-$Ala_{0.21}$-LDHs, $Mg_{1.78}$/Al-$Leu_{0.22}$-LDHs, $Mg_{2.03}$/Al-$Phe_{0.79}$-LDHs, $Mg_{2.22}$/Al-$Tyr_{0.71}$-LDHs, $Mg_{2.03}$/Al-Me-$Phe_{0.97}$-LDHs, $Mg_{2.70}$/Al-$Pro_{0.26}$-LDHs, $Mg_{2.70}$/Al-Me-$Pro_{0.26}$-LDHs, $Ca_{2.03}$/Al-$Phe_{0.64}$-LDHs, $Ni_{1.78}$/Al-$Phe_{0.97}$-LDHs, and $Zn_{1.86}$/Al-$Phe_{0.66}$-LDHs. Increasing the intercalated amounts of L-proline anions from 26% ($Mg_{2.70}$/Al-$Pro_{0.26}$-LDHs) to 33% ($Mg_{2.70}$/Al-$Pro_{0.33}$-LDHs) altered the electrostatic interactions between L-proline anions and brucite-like layer from monodentate to bidentate mode, though the interlayer L-proline anions remained in a monolayer horizontal arrangement.

3.2. Effects of LDH nanosheets on amine-catalyzed asymmetric epoxidation of α, β-unsaturated aldehyde

The L-proline anions intercalated in LDHs was first applied in the asymmetric epoxidation of cinnamaldehyde. As shown in Table 1, 94% conversion of cinnamaldehyde and 70% yield of glycidaldehyde (isolated yield of 67%) were obtained in 3 h on $Mg_{2.70}$/Al-$Pro_{0.33}$-LDHs (entry 1). Partly hydrolysis of cinnamaldehyde was observed as a side reaction, producing benzaldehyde as byproduct, which has been reported previously [98–102], accounting for the yield inferior to the conversion (a selectivity of 74%). In 2 h (entry 2), 82% cinnamaldehyde conversion and 54% epoxide yield were afforded. Prolonging the reaction time to 4 h (entry 3), 98% cinnamaldehyde conversion and 72% epoxide yield were afforded. The similar cinnamaldehyde conversion, epoxide yield, and ee value were reached in 3 h and 4 h. Decreasing the amount of $Mg_{2.70}$/Al-$Pro_{0.33}$-LDHs in half (5 mol% amino acid anions), 78% cinnamaldehyde conversion and 40% epoxide yield were afforded (entry 4). So it is obvious that L-proline anions intercalated in LDHs are efficient catalysts for epoxidation of cinnamaldehyde. No epoxidation reaction occurred in the absence of L-proline anion (entry 5), indicating that the –NH- in the L-proline anion was the catalytic center. With L-proline sodium salt as the catalyst (entry 6), 67% conversion was afforded, but with only an epoxide yield of 7%. No epoxide was produced with L-proline ethylester (entry 7) or L-proline (entry 8) as catalyst, although a 20% or 10% cinnamaldehyde conversion was afforded. By adding 10 mol% NaOH together with L-proline sodium salt as the catalyst (entry 9), the epoxide yield increased from 7% to 22% with a cinnamaldehyde conversion of 60%, revealing that the epoxide yield was improved with increasing basicity. But a lower epoxide yield was achieved with L-proline sodium salt together with 10 mol% NaOH than with intercalated L-proline anions. The better conversion of cinnamaldehyde to its epoxide with $Mg_{2.70}$/Al-$Pro_{0.33}$-LDHs than with L-proline sodium salt revealed that the LDH nanosheets afforded the desired basicity more effectively to activate the oxidant, facilitating the attack of HOO^- to the carbon–carbon double bonds in the iminium intermediate, and the epoxidation dominated. But the LDH nanosheets with the L-proline anion just simply adsorbed on the exterior surface (entry 10) were invalid to promote the epoxidation, affording only an epoxide yield of <5% under 58% conversion, similar to the case with L-proline sodium salt. It is the nanosheets with amine sites encapsulated in the interlayer regions that function synergically as solid base to facilitate the activation of oxidant and the subsequent nucleophilic attack. With $Mg_{2.70}$/Al-$Pro_{0.26}$-LDHs as catalyst (entry 11), in which the electrostatic interactions between L-proline anions and brucite-like layer are monodentate mode, 96% conversion of cinnamaldehyde and 76% yield of glycidaldehyde were obtained. $Mg_{2.70}$/Al-$Pro_{0.33}$-LDHs (entry 1) and $Mg_{2.70}$/Al-$Pro_{0.26}$-LDHs (entry 11) afforded similar cinnamaldehyde conversion and epoxide yield, indicating that the bidentate or monodentate interactions impose no visible effects on the synergy of LDH nanosheets with intercalated amine sites.

Simple small primary amines are generally inferior to secondary amines in the catalytic activity due to unfavorable imine-enamine equilibria [103–105]. But promotion of cinnamaldehyde conversion and epoxide yield was observed in this work by intercalating primary amines in LDHs. As shown in Table 1, the conversion of cinnamaldehyde increased from 30% for Me-Phe-Na to 88% for

Table 1
Catalytic asymmetric epoxidation of α, β-unsaturated aldehydes[a].

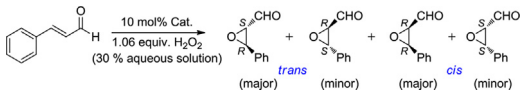

Entry	Catalyst	Time (h)	Conversion of aldehyde (%)[b]	^{1}H NMR yield (%)[b]	Selectivity to epoxide (%)	dr[b] (trans/cis)	ee of *trans* (%)[c]	ee of *cis* (%)[c]
1	$Mg_{2.70}$/Al-$Pro_{0.33}$-LDHs	3	94	70/67[d]	74	83:17	93	70
2	$Mg_{2.70}$/Al-$Pro_{0.33}$-LDHs	2	82	54	65	78:22	90	73
3	$Mg_{2.70}$/Al-$Pro_{0.33}$-LDHs	4	98	72	73	81:19	95	62
4	$Mg_{2.70}$/Al-$Pro_{0.33}$-LDHs[e]	3	78	40	51	75:25	92	71
5	Mg/Al-CO_3^{2-}-LDHs	3	0	0	0	ND[f]	ND	ND
6	Pro-Na	3	67	7	10	70:30	0	0
7	Pro ethylester	3	20	0	0	ND	ND	ND
8	Pro	3	10	0	0	ND	ND	ND
9	Pro-Na + NaOH[g]	3	60	22	37	82:18	0	0
10	Pro/Mg/Al-CO_3^{2-}-LDHs	3	58	<5	<9	70:30	39	58
11	$Mg_{2.70}$/Al-$Pro_{0.26}$-LDHs	3	96 (94)	76 (72)	79 (77)	82:18 (83:17)	93 (91)	78 (73)
12	$Mg_{2.03}$/Al-Me-$Phe_{0.97}$-LDHs	4	88 (90)	60 (58)	68 (64)	73:27 (76:24)	28 (27)	11 (10)
13	$Mg_{2.03}$/Al-$Phe_{0.79}$-LDHs	4	82 (80)	48 (46)	59 (58)	81:19 (79:21)	44 (42)	17 (17)
14	$Mg_{1.78}$/Al-$Leu_{0.22}$-LDHs	4	80 (78)	42 (40)	52 (51)	75:25 (76:24)	42 (40)	17 (17)
15	$Mg_{2.22}$/Al-$Tyr_{0.71}$-LDHs	4	62 (64)	32 (32)	52 (50)	76:24 (75:25)	38 (38)	18 (17)
16	$Mg_{2.03}$/Al-$Ala_{0.21}$-LDHs	4	60 (60)	26 (26)	43 (43)	77:23 (77:23)	36 (35)	19 (20)
17	$Mg_{2.03}$/Al-$Ser_{0.21}$-LDHs	4	52 (54)	20 (18)	38 (33)	75:25 (78:22)	27 (27)	24 (24)
18	$Ca_{2.03}$/Al-$Phe_{0.64}$-LDHs	4	92	58	63	72:28	42	32
19	$Ni_{1.78}$/Al-$Phe_{0.97}$-LDHs	4	48	14	29	86:14	31	18
20	$Zn_{1.86}$/Al-$Phe_{0.66}$-LDHs	4	30	5	17	80:20	36	28
21	$Mg_{2.70}$/Al-Me-$Pro_{0.26}$-LDHs	3	92	74	80	83:17	63	79

$Mg_{2.03}$/Al-Me-$Phe_{0.97}$-LDHs (entry 12), from 34% for Phe-Na to 82% for $Mg_{2.03}$/Al-$Phe_{0.79}$-LDHs (entry 13), from 38% for Leu-Na to 78% for $Mg_{1.78}$/Al-$Leu_{0.22}$-LDHs (entry 14), from 22% for Tyr-Na to 62% for $Mg_{2.22}$/Al-$Tyr_{0.71}$-LDHs (entry 15), from 26% for Ala-Na to 60% for $Mg_{2.03}$/Al-$Ala_{0.21}$-LDHs (entry 16), and from 32% for Ser-Na to 52% for $Mg_{2.03}$/Al-$Ser_{0.21}$-LDHs (entry 17). But the yields of glycidaldehyde were only observed with LDH nanosheets-attached amines (entries 12, 13, 14, 15, 16, and 17). Only trace or no epoxide was observed with Me-Phe-Na, Phe-Na, Leu-Na, Tyr-Na, Ala-Na, and Ser-Na. Similar to the case with intercalated secondary amine, the basicity provided by the LDH nanosheets could facilitate the epoxidation on the primary amine sites, affording the selectivity to epoxide. The dependence of epoxide selectivity on the basicity of brucite-like layers further proves the assistance of LDH nanosheets as a solid base. For $Ca_{2.03}$/Al-$Phe_{0.64}$-LDHs, with a higher basicity than $Mg_{2.03}$/Al-$Phe_{0.79}$-LDHs, 63% selectivity (92% conversion and 58% yield) was observed (entry 18). For $Ni_{1.78}$/Al-$Phe_{0.97}$-LDHs, with a lower basicity than $Mg_{2.03}$/Al-$Phe_{0.79}$-LDHs, 29% selectivity (48% conversion and 14% yield) was observed (entry 19). For $Zn_{1.86}$/Al-$Phe_{0.66}$-LDHs, with a lower basicity than $Ni_{1.78}$/Al-$Phe_{0.97}$-LDHs, 17% selectivity (30% conversion and 5% yield) was observed (entry 20). The observations in this work are sustained by our previous work [106], where the improvement of catalytic activity has been achieved by using ligand-attached LDH nanosheets to afford the desired basicity in Rh(III)-catalyzed C—H activation reaction.

The LDH nanosheets play a more critical role in improving the ee of glycidaldehyde, as can be clearly seen from entry 1 and entry 8. With $Mg_{2.70}$/Al-$Pro_{0.33}$-LDHs, 93% ee for major diastereomer (*trans*) was achieved, while no ee was observed with L-proline sodium salt. 39% ee for major diastereomer (*trans*) was produced (entry 10) even with the L-proline anion just simply adsorbed on the exterior surface of Mg/Al-CO_3^{2-}-LDHs, demonstrating that the enantioselective enhancement originated from LDHs nanosheets, and the enhancement was especially obvious with the amine sites located at the interlayer regions of LDHs. Even for primary amines, with acyclic structure and thus difficult to produce enantioselectivity, the ee was also evoked by the attachment of LDH nanosheets. 28% ee for major diastereomer was afforded with $Mg_{2.03}$/Al-Me-$Phe_{0.97}$-LDHs (entry 12), 44% ee with $Mg_{2.03}$/Al-$Phe_{0.79}$-LDHs (entry 13), 42% ee with $Mg_{1.78}$/Al-$Leu_{0.22}$-LDHs (entry 14), 38% ee with $Mg_{2.22}$/Al-$Tyr_{0.71}$-LDHs (entry 15), 36% ee with $Mg_{2.03}$/Al-$Ala_{0.21}$-LDHs (entry 16), and 27% ee with $Mg_{2.03}$/Al-$Ser_{0.21}$-LDHs (entry 17). The LDH nanosheets are supposed to supply the desired steric hindrance around the amine sites as attached rigid planer substituent, and direct the access trajectory of activated oxidant to the carbon–carbon double bond in the iminium intermediate. The observations in this work are sustained by our previous work [107,108], where the boosting of enantioselectivity has been achieved by using LDH nanosheets as the rigid planer substituent in both organometallic-catalyzed epoxidation and organo-catalyzed aldol addition reaction. The Jørgensen-Hayashi catalyst, ((2*S*)-2-[Bis[3,5-bis(trifluoromethyl)phenyl](trimethyl- siloxy)methyl]pyrrolidine) [60], which was known as the most successful organocatalyst and very related to the amino acid system in our work, has been evaluated under our reaction condition, affording 80% cinnamaldehyde conversion, 62% glycidaldehyde yield, and 93% ee for major diastereomer (trans). The heterogeneous catalyst in our work, $Mg_{2.70}$/Al-$Pro_{0.33}$-LDHs, is comparable to the homogeneous system in both yield and ee. Using organic peroxides *m*-chloro perbenzoic (*m*-CPBA) as oxidant, <5% cinnamaldehyde conversion with no epoxide yield was produced with Pro-Na, Pro ethylester, or $Mg_{2.70}$/Al-$Pro_{0.33}$-LDHs as catalysts. *m*-CPBA was unlikely an efficient oxidant in amino acid systems, consistent with the results reported by the literature with Jørgensen-Hayashi catalyst [60].

The substrate scope for $Mg_{2.70}$/Al-$Pro_{0.26}$-LDHs-catalyzed asymmetric epoxidation of α, β-unsaturated aldehydes was then explored (Table 2). For aromatic aldehydes, both electron-withdrawing and electron-donating substituents were well tolerated. In 3 h, > 99% conversion, 32% epoxide yield, and 89% ee for *trans* isomer were obtained for the asymmetric epoxidation

Table 2
Substrate scope for $Mg_{2.70}$/Al-$Pro_{0.26}$-LDHs-catalyzed asymmetric epoxidation of α, β-unsaturated aldehydes[a].

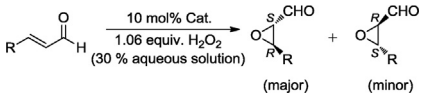

Entry	Substrate	Conversion of aldehyde (%)[b]	^{1}H NMR Yield (%)[b]	Isolated yield of epoxide aldehyde (%)[c]	Selectivity (%)	ee of trans isomer[d] (%)
1	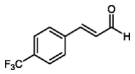	>99 (>99)	32 (34)	30	32 (34)	89 (89)
2	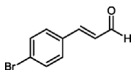	86 (88)	44 (42)	40	51 (48)	96 (96)
3	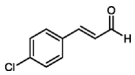	90 (86)	48 (46)	45	53 (53)	94 (95)
4	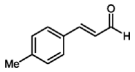	72 (70)	44 (40)	40	61 (57)	88 (88)
5[e]	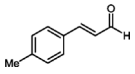	96	60	57	62	89
6[e]		96 (94)	62 (62)	ND (ND)[f]	64 (66)	77[g]

[a] Reaction conditions: 0.25 mmol of α, β-unsaturated aldehydes, 1.06 equiv. of H_2O_2 in 30% aqueous solution, 10 mol% of α-amino acid anions, 1 mL of acetone, 25 °C, 3 h of reaction time.
[b] Determined by ^{1}H NMR using dimethyl maleate as internal standard after reduced by $NaBH_4$.
[c] All the isolated yields were consistent with the ^{1}H NMR yield.
[d] Determined by HPLC analysis on chiral OD-H or OJ-H column after reduced by $NaBH_4$.
[e] 5 h of reaction time.
[f] Not Determined due to the volatility of the product, the 3-isopropyl-oxirane-2-carbaldehyde cannot be isolated.
[g] Determined by Mosher's MTPA method. The figures in the parenthesis are reproduced results.

of 4-trifluoromethyl-cinnamaldehyde (entry 1); 86% conversion, 44% epoxide yield, and 96% ee were obtained for 4-bromo-cinnamaldehyde (entry 2); 90% conversion, 48% epoxide yield, and 94% ee were obtained for 4-chloro-cinnamaldehyde (entry 3); 72% conversion, 44% epoxide yield, and 88% ee were obtained for 4-methyl-cinnamaldehyde (entry 4). With increasing electron-donating effects, the aromatic aldehydes were more difficult to be activated. It is very likely that the electron-withdrawing substituents decrease the electron density of the carbon–carbon double bond, making the carbon–carbon double bond susceptible to being nucleophilically attacked. While the electron-donating substituents increase the electron density of the carbon–carbon double bond, making the nucleophilic attack of carbon–carbon double bond more difficult. But by prolonging the reaction time to 5 h, 96% conversion, 60% epoxide yield, and 89% ee were obtained for 4-methyl-cinnamaldehyde (entry 5). Then the aldehydes were extended from aromatic aldehydes to aliphatic aldehyde. 96% conversion, 62% epoxide yield, and 77% ee were observed in 5 h for the β-disubstituted α, β-unsaturated aldehyde (4-methyl butenal) (entry 6). With an attempt to further extend the substrate generality, the asymmetric epoxidation of 2H-chromene-3-carbaldehyde, *trans*-4-phenyl-3-buten-2-one, *trans*-methyl-cinnamate, *trans*-cinnamonitrile, and *trans*-3-(2-furyl)acrolein was also examined. Unfortunately, no reaction occurred. The development of more effective catalysts for more extensive substrates merits further efforts.

3.3. Influence of hydrophobicity and ordered arrangement of interlayer amines on catalytic efficacy

It is interesting that, the primary amines without attachment to LDH nanosheets provided similar cinnamaldehyde conversion (in the range of 22% to 38%), but as can be seen from Table 1, those with LDH nanosheet attached afforded a conversion changing from 52% to 88%. The epoxide yields on LDH nanosheets-attached primary amines also differ greatly from each other (from 20%–60%). That means the catalytic activities of primary amines might be affected by the interlayer microenvironment. The interlayer hydrophobicity was then explored by the fluorescence spectra of pyrene molecules, which were encapsulated in the interlayer of amine-intercalated LDHs. The vibronic structure of pyrene is known to be sensitive to the polarity of the environment [109–114]. The ratio of the fluorescence intensity of the first to the third vibronic peaks (I_{373}/I_{384}) increased from ~0.6 to ~2.0 with the increasing polarity of the environment [115,116]. The I_{373}/I_{384} was 1.43 for $Mg_{2.03}$/Al-$Ser_{0.21}$-LDHs, 1.34 for $Mg_{2.03}$/Al-$Ala_{0.21}$-LDHs, 1.30 for $Mg_{1.78}$/Al-$Leu_{0.22}$-LDHs, and 1.20 for $Mg_{2.03}$/Al-$Phe_{0.79}$-LDHs (Fig. 2A), revealing that the interlayer hydrophobicity gradually increased. With increasing interlayer hydrophobicity, the cinnamaldehyde conversion and epoxide yield were improved (Fig. 2A). The hydrophobicity was further tailored by changing the substituent on the aromatic ring (Fig. 2B). With a 4-hydroxyl substituent on the aromatic ring, the I_{373}/I_{384} was 1.32 ($Mg_{2.22}$/Al-$Tyr_{0.71}$-LDHs). With a 4-methyl substituent on the aromatic ring, the I_{373}/I_{384} was 1.07 ($Mg_{2.03}$/Al-Me-$Phe_{0.97}$-LDHs). The cinnamaldehyde conversion and epoxide yield were also observed to increase with increasing interlayer hydrophobicity (Fig. 2B). For LDH nanosheets-attached proline based amine, the hydrophobicity was also tailored by substituting the H atom in 2-C of L-proline with methyl group. The I_{373}/I_{384} was 1.40 for $Mg_{2.70}$/Al-$Pro_{0.26}$-LDHs and 1.37 for $Mg_{2.70}$/Al-Me-$Pro_{0.26}$-LDHs. $Mg_{2.70}$/Al-Me-$Pro_{0.26}$-LDHs (Table 1, Entry 21) afforded 92% cinnamaldehyde conversion and 74% epoxide yield, similar to $Mg_{2.70}$/Al-$Pro_{0.26}$-LDHs (96% cinnamaldehyde conversion and 76% epoxide yield (Table 1, Entry 11)). The slight difference of hydrophobicity between the $Mg_{2.70}$/Al-$Pro_{0.26}$-LDHs and

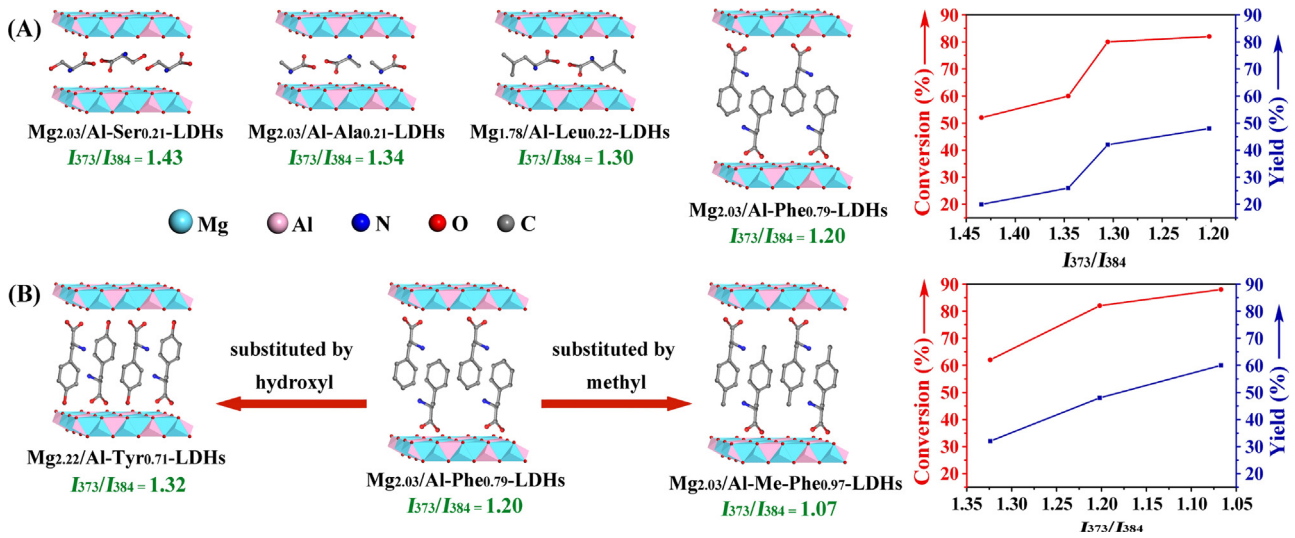

Fig. 2. The interlayer hydrophobic microenvironment and its influence on the conversion and epoxide yield. In the schematic illustration of intercalated LDHs, the H atoms have been omitted.

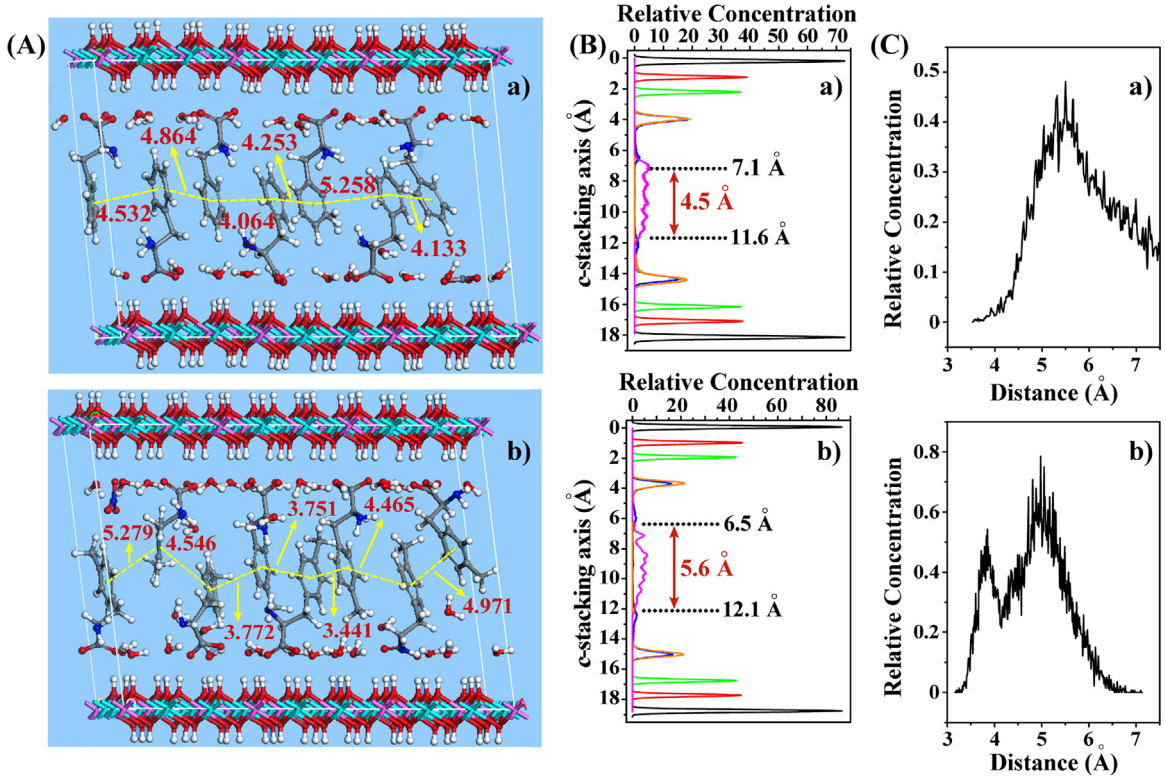

Fig. 3. (A) Side view of the simulated arrangement of interlayer α-amino acid anions, carbonate ion (or nitrate ion), and water molecules, (B) Atomic density profiles along the *c*-stacking axis (the black line represents Mg atoms in the LDHs layer, the red line represents O atoms in the LDHs layer, the green line represents H atoms in the LDHs layer, the blue line represents O atoms in the water molecules, the orange line represents O atoms in the α-amino acid anions, and the magenta line represents C atoms of the phenyl rings in the α-amino acid anions), and (C) the distribution of distance between two adjacent centroids of the phenyl rings for a) $Mg_{2.03}$/Al-$Phe_{0.79}$-LDHs and b) $Mg_{2.03}$/Al-Me-$Phe_{0.97}$-LDHs. (For interpretation of the references to color in this figure legend, the reader is referred to the web version of this article.)

the $Mg_{2.70}$/Al-Me-$Pro_{0.26}$-LDHs make no visible effects on the cinnamaldehyde conversion and epoxide yield.

The observed enantioselectivites were then related to the interlayer hydrophobicity. For intercalated primary amines, the ee was improved with increasing interlayer hydrophobicity. But an exception arose for $Mg_{2.03}$/Al-Me-$Phe_{0.97}$-LDHs, which afforded a lower ee with a stronger interlayer hydrophobicity than other investigated catalysts. Similarly, for intercalated proline based amine, more hydrophobic $Mg_{2.70}$/Al-Me-$Pro_{0.26}$-LDHs (Table 1, Entry 21) afforded 63% ee, lower than the ee (93% as shown in Table 1, Entry 11) afforded by less hydrophobic $Mg_{2.70}$/Al-$Pro_{0.26}$-LDHs. So the interlayer arrangement of intercalated amines was studied, and then related to the ee of epoxide. The arrangement of interlayer anions in $Mg_{2.03}$/Al-$Phe_{0.79}$-LDHs and $Mg_{2.03}$/Al-Me-$Phe_{0.97}$-LDHs was simulated by molecular dynamics (MD) (Fig. 3). According to the side view of the simulated arrangement of interlayer anions and water molecules (Fig. 3A), Mg, O, and H atoms in the brucite-like layer along the *c*-stacking axis were profiled

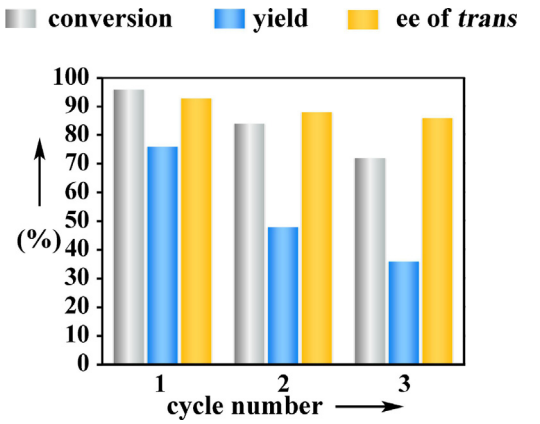

Fig. 4. Reusability of $Mg_{2.70}$/Al-$Pro_{0.26}$-LDHs catalyst in asymmetric epoxidation of cinnamaldehyde.

(Fig. 3B) at 0.2 and 18.1 Å, 1.2 and 17.1 Å, and 2.2 and 16.2 Å for $Mg_{2.03}$/Al-$Phe_{0.79}$-LDHs, and at 0 and 18.7 Å, 1.0 and 17.7 Å, and 1.9 and 16.8 Å for $Mg_{2.03}$/Al-Me-$Phe_{0.97}$-LDHs. The O atoms in interlayer water molecules and α-amino acid anions were profiled at 4.0 Å and 14.4 Å for $Mg_{2.03}$/Al-$Phe_{0.79}$-LDHs, and 3.7 Å and 15.0 Å for $Mg_{2.03}$/Al-Me-$Phe_{0.97}$-LDHs. The profile distance between the O atoms in interlayer water/anions and the H atoms in the OH groups of brucite-like layers is estimated as 1.8 Å for both $Mg_{2.03}$/Al-$Phe_{0.79}$-LDHs and $Mg_{2.03}$/Al-Me-$Phe_{0.97}$-LDHs, which is consistent with the binding length of hydrogen bonds. The C atoms in the phenyl rings of interlayer α-amino acid anions are profiled at 7.1-11.6 Å for $Mg_{2.03}$/Al-$Phe_{0.79}$-LDHs and 6.5-12.1 Å for $Mg_{2.03}$/Al-Me-$Phe_{0.97}$-LDHs. The distribution range of the phenyl rings along the *c*-stacking axis was 4.5 Å for $Mg_{2.03}$/Al-$Phe_{0.79}$-LDHs and 5.6 Å for $Mg_{2.03}$/Al-Me-$Phe_{0.97}$-LDHs. The narrower distribution range of phenyl rings in $Mg_{2.03}$/Al-$Phe_{0.79}$-LDHs than that in $Mg_{2.03}$/Al-Me-$Phe_{0.97}$-LDHs revealed that the arrangement of interlayer L-phenylalanine anions was less stagger than interlayer 4-methy-L-phenylalanine anions. The distance between two adjacent centroids of phenyl ring along *ab*-plane (Fig. 3C) is estimated from Fig. 3A with the maximum at 5.5 Å for $Mg_{2.03}$/Al-$Phe_{0.79}$-LDHs, and at 3.8 Å to 5.0 Å for $Mg_{2.03}$/Al-Me-$Phe_{0.97}$-LDHs. Both of the profile distance along *c*-stacking axis and *ab*-plane indicate that the arrangement of interlayer L-phenylalanine anions is better ordered than that of interlayer 4-methy-L-phenylalanine anions, accounting for the enhancement of ee in the asymmetric epoxidation.

3.4. Catalyst reusability

The secondary amine intercalated Mg/Al-LDHs catalyst has been recycled and reused without any treatment. On $Mg_{2.70}$/Al-$Pro_{0.26}$-LDHs (Fig. 4), the cinnamaldehyde conversion and epoxide yield declined in the recycles. As discussed above, the electrostatic interactions between interlayer L-proline anions and brucite-like layer are monodentate mode for $Mg_{2.70}$/Al-$Pro_{0.26}$-LDHs, which was not strong enough to prevent the amine leaching. But the ee was well preserved in the recycle runs. On $Mg_{2.70}$/Al-$Pro_{0.33}$-LDHs (Fig. 5), 93% ee was also well preserved in ten cycles. The cinnamaldehyde conversion and epoxide yield were well maintained in eight cycles. Visible decline of cinnamaldehyde conversion and epoxide yield was only observed in the last two cycles due to the slight leaching of interlayer amines (Table S2). That means the bidentate electrostatic interactions could effectively hold the interlayer L-proline anions attached to the brucite-like layer.

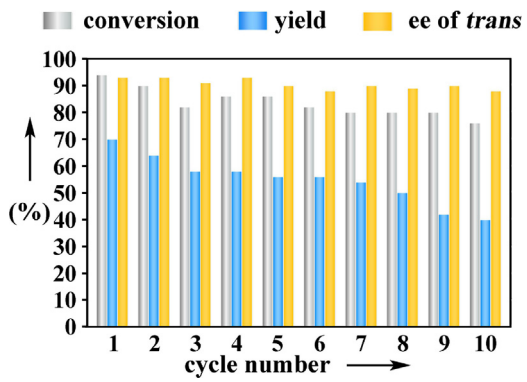

Fig. 5. Reusability of $Mg_{2.70}$/Al-$Pro_{0.33}$-LDHs catalyst in asymmetric epoxidation of cinnamaldehyde.

4. Conclusions

In conclusion, the amine-catalyzed asymmetric epoxidation of α, β-unsaturated aldehydes was promoted by attaching to LDH nanosheets. 76% of epoxide yield and 93% ee for major diastereomer have been achieved in the asymmetric epoxidation of cinnamaldehyde. The strategy of attaching amines to LDH nanosheets proves versatile and viable to facilitate the asymmetric epoxidation of α, β-unsaturated aldehydes. The catalytic activity was enhanced by the basicity of LDH nanosheets and further improved by increasing hydrophobicity of interlayer amines. The enantioselectivity was boosted by the steric synergies of LDH nanosheets and further improved by better ordered arrangement of interlayer amines. Nevertheless, there remain great challenges that are worth of further in-depth investigation. One is how to inhibit the leaching of interlayer anions. The non-covalent interactions (electrostatic interaction, H-bonding interaction, and etc) between LDH nanosheets and interlayer amines are superior in the preservation of original asymmetric environment, yet are not strong enough to resist the exchange by ambient anions. The other is how to ameliorate the efficacy of heterogeneous asymmetric catalysis. The amine-intercalated LDHs in our work are inefficient for more challenging substrates, such as α, β-unsaturated ketones, α, β-unsaturated esters, and α, β-unsaturated nitriles.

Acknowledgements

Financial supports by NSFC (No. 21673016) and 973 Project (2014CB932101) are gratefully acknowledged.

Appendix A. Supplementary data

Supplementary data associated with this article can be found, in the online version, at http://dx.doi.org/10.1016/j.mcat.2017.09.035.

References

[1] M.M. Faul, B.E. Huff, Chem. Rev. 100 (2000) 2407–2474.
[2] K.B. Sharpless, Angew. Chem. Int. Ed. 41 (2002) 2024–2032.
[3] C. Bonini, G. Righi, Tetrahedron 58 (2002) 4981–5021.
[4] M.M. Heravi, T.B. Lashaki, N. Poorahmad, Tetrahedron: Asymmetry 26 (2015) 405–495.
[5] M. Brichacek, L.A. Batory, J.T. Njardarson, Angew. Chem. Int. Ed. 49 (2010) 1648–1651.
[6] T. Nemoto, T. Ohshima, M. Shibasaki, Tetrahedron Lett. 41 (2000) 9569–9574.
[7] L. Carde, H. Davies, T.P. Geller, S.M. Roberts, Tetrahedron Lett. 40 (1999) 5421–5424.
[8] K. Kato, M. Ono, H. Akita, Tetrahedron Lett. 38 (1997) 1805–1808.
[9] Y. Qian, X. Xu, L. Jiang, D. Prajapati, W. Hu, J. Org. Chem. 75 (2010) 7483–7486.

[10] T.K.M. Shing, T. Luk, C.M. Lee, Tetrahedron 62 (2006) 6621–6629.
[11] T. Yamaguchi, N. Harada, K. Ozaki, T. Hashiyama, Tetrahedron Lett. 39 (1998) 5575–5578.
[12] H. Pellissier, in: M. Todd (Ed.), Separation of Enantiomers, Synthetic Method, Wiley-VCH, Weinheim, 2014, pp. 75–122.
[13] J.F. Larrow, P.F. Quigley, Industrial applications of the jacobsen hydrolytic kinetic resolution technology, in: E.M. Carreira, H. Yamamoto (Eds.), Comprehensive Chirality, vol. 9, Elsevier, Amsterdam, 2012, pp. 129–146.
[14] H. Pellissier, Adv. Synth. Catal. 353 (2011) 1613–1666.
[15] W.J. Choi, Appl. Microbiol. Biotechnol. 84 (2009) 239–247.
[16] J.M. Keith, J.F. Larrow, E.N. Jacobsen, Adv. Synth. Catal. 343 (2001) 5–26.
[17] Z. Li, H. Yamamoto, Acc. Chem. Res. 46 (2013) 506–518.
[18] A.U. Barlan, W. Zhang, H. Yamamoto, Tetrahedron 63 (2007) 6075–6087.
[19] E.M. McGarrigle, D.G. Gilheany, Chem. Rev. 105 (2005) 1563–1602.
[20] T. Katsuki, K.B. Sharpless, J. Am. Chem. Soc. 102 (1980) 5974–5976.
[21] W. Zhang, J.L. Loebach, S.R. Wilson, E.N. Jacobsen, J. Am. Chem. Soc. 112 (1990) 2801–2803.
[22] Y. Tanaka, K. Nishimura, K. Tomioka, Tetrahedron 59 (2003) 4549–4556.
[23] O. Jacques, S.J. Richards, R.F.W. Jackson, Chem. Commun. (2001) 2712–2713.
[24] C.L. Elston, R.F.W. Jackson, S.J.F. MacDonald, P.J. Murray, Angew. Chem. Int. Ed. 36 (1997) 410–412.
[25] Y. Chu, X. Liu, W. Li, X. Hu, L. Lin, X. Feng, Chem. Sci. 3 (2012) 1996–2000.
[26] A.R. Keeri, I. Justyniak, J. Jurczak, J. Lewiński, Adv. Synth. Catal. 358 (2016) 864–868.
[27] M. Kubisiak, K. Zelga, I. Justyniak, E. Tratkiewicz, T. Pietrzak, A.R. Keeri, Z. Ochal, L. Hartenstein, P.W. Roesky, J. Lewiński, Organometallics 32 (2013) 5263–5265.
[28] R. Infante, Y. Hernández, J. Nieto, C. Andrés, Eur. J. Org. Chem. (2013) 4863–4869.
[29] H. Wang, Z. Wang, K. Ding, Tetrahedron Lett. 50 (2009) 2200–2203.
[30] A. Minatti, K.H. Dötz, Eur. J. Org. Chem. (2006) 268–276.
[31] A. Minatti, K.H. Dötz, Synlett 9 (2004) 1634–1636.
[32] O. Cussó, M. Cianfanelli, X. Ribas, R.J.M. Klein Gebbink, M. Costas, J. Am. Chem. Soc. 138 (2016) 2732–2738.
[33] W. Dai, G. Li, B. Chen, L. Wang, S. Gao, Org. Lett. 17 (2015) 904–907.
[34] O.Y. Lyakin, A.M. Zima, D.G. Samsonenko, K.P. Bryliakov, E.P. Talsi, ACS Catal. 5 (2015) 2702–2707.
[35] O. Cussó, I. Garcia-Bosch, X. Ribas, J. Lloret-Fillol, M. Costas, J. Am. Chem. Soc. 135 (2013) 14871–14878.
[36] Y. Wang, D. Janardanan, D. Usharani, K. Han, L. Que Jr., S. Shaik, ACS Catal. 3 (2013) 1334–1341.
[37] B. Wang, S. Wang, C. Xia, W. Sun, J. Chem. Eur. 18 (2012) 7332–7335.
[38] O.Y. Lyakin, K.P. Bryliakov, E.P. Talsi, Inorg. Chem. 50 (2011) 5526–5538.
[39] Y. Nishikawa, H. Yamamoto, J. Am. Chem. Soc. 133 (2011) 8432–8435.
[40] M. Wu, C. Miao, S. Wang, X. Hu, C. Xia, F.E. Kühn, W. Sun, Adv. Synth. Catal. 353 (2011) 3014–3022.
[41] R. Mas-Ballesté, L. Que Jr., J. Am. Chem. Soc. 129 (2007) 15964–15972.
[42] Q. Qian, Y. Tan, B. Zhao, T. Feng, Q. Shen, Y. Yao, Org. Lett. 16 (2014) 4516–4519.
[43] S.A. Schuetz, E.A. Bowman, C.M. Silvernail, V.W. Day, J.A. Belot, J. Organomet. Chem. 690 (2005) 1011–1017.
[44] H. Kakei, R. Tsuji, T. Ohshima, M. Shibasaki, J. Am. Chem. Soc. 127 (2005) 8962–8963.
[45] S. Matsunaga, T. Kinoshita, S. Okada, S. Harada, M. Shibasaki, J. Am. Chem. Soc. 126 (2004) 7559–7570.
[46] T. Nemoto, H. Kakei, V. Gnanadesikan, S. Tosaki, T. Ohshima, M. Shibasaki, J. Am. Chem. Soc. 124 (2002) 14544–14545.
[47] R. Chen, C. Qian, J.G. de Vries, Tetrahedron Lett. 42 (2001) 6919–6921.
[48] T. Nemoto, T. Ohshima, K. Yamaguchi, M. Shibasaki, J. Am. Chem. Soc. 123 (2001) 2725–2732.
[49] Y. Zhu, Q. Wang, R.G. Cornwall, Y. Shi, Chem. Rev. 114 (2014) 8199–8256.
[50] R.L. Davis, J. Stiller, T. Naicker, H. Jiang, K.A. Jørgensen, Angew. Chem. Int. Ed. 53 (2014) 7406–7426.
[51] D.W.C. MacMillan, Nature 455 (2008) 304–308.
[52] Y. Shi, Acc. Chem. Res. 37 (2004) 488–496.
[53] S. Shirakawa, K. Maruoka, Angew. Chem. Int. Ed. 52 (2013) 4312–4348.
[54] T. Ooi, K. Maruoka, Angew. Chem. Int. Ed. 46 (2007) 4222–4266.
[55] S.S. Jew, J.H. Lee, B.S. Jeong, M.S. Yoo, M.J. Kim, Y.J. Lee, J. Lee, S.H. Choi, K. Lee, M.S. Lah, H.G. Park, Angew. Chem. Int. Ed. 44 (2005) 1383–1385.
[56] T. Ooi, D. Ohara, M. Tamura, K. Maruoka, J. Am. Chem. Soc. 126 (2004) 6844–6845.
[57] C.E. Jakobsche, G. Peris, S.J. Miller, Angew. Chem. Int. Ed. 47 (2008) 6707–6711.
[58] G. Peris, C.E. Jakobsche, S.J. Miller, J. Am. Chem. Soc. 129 (2007) 8710–8711.
[59] D.A. Singleton, Z. Wang, J. Am. Chem. Soc. 127 (2005) 6679–6685.
[60] M. Marigo, J. Franzén, T.B. Poulsen, W. Zhuang, K.A. Jørgensen, J. Am. Chem. Soc. 127 (2005) 6964–6965.
[61] O. Lifchits, M. Mahlau, C.M. Reisinger, A. Lee, C. Farès, I. Polyak, G. Gopakumar, W. Thiel, B. List, J. Am. Chem. Soc. 135 (2013) 6677–6693.
[62] O. Lifchits, C.M. Reisinger, B. List, J. Am. Chem. Soc. 132 (2010) 10227–10229.
[63] A. Russo, A. Lattanzi, Eur J. Org. Chem. (2008) 2767–2773.
[64] M.P. Paudyal, N.P. Rath, C.D. Spilling, Org. Lett. 12 (2010) 2954–2957.
[65] K. Kato, M. Ono, H. Akita, Tetrahedron 57 (2001) 10055–10062.
[66] K. Akagawa, T. Hirata, K. Kudo, Synlett 27 (2016) 1217–1222.
[67] H. Kawai, S. Okusu, Z. Yuan, E. Tokunaga, A. Yamano, M. Shiro, N. Shibata, Angew. Chem. Int. Ed. 52 (2013) 2221–2225.
[68] D.K. Romney, S.J. Miller, Org. Lett. 14 (2012) 1138–1141.
[69] S. Juliá, J. Masana, Angew. Chem. Int. Ed. 19 (1980) 929–931.
[70] A. Capobianco, A. Russo, A. Lattanzi, A. Peluso, Adv. Synth. Catal. 354 (2012) 2789–2796.
[71] A. Lattanzi, Adv. Synth. Catal. 348 (2006) 339–346.
[72] A. Lattanzi, Org. Lett. 7 (2005) 2579–2582.
[73] K. Akagawa, K. Kudo, Adv. Synth. Catal. 353 (2011) 843–847.
[74] D. Tichit, D. Lutic, B. Coq, R. Durand, R. Teissier, J. Catal. 219 (2003) 167–175.
[75] S. He, Z. An, M. Wei, D.G. Evans, X. Duan, Chem. Commun. 49 (2013) 5912–5920.
[76] R. Manivannan, A. Pandurangan, Appl. Clay Sci. 44 (2009) 137–143.
[77] M.J. Climent, A. Corma, S. Iborra, A. Velty, J. Catal. 221 (2004) 474–482.
[78] S. Aisawa, S. Takahashi, W. Ogasawara, Y. Umetsu, E. Narita, J. Solid State Chem. 162 (2001) 52–62.
[79] N.T. Whilton, P.J. Vickers, S. Mann, J. Mater. Chem. 7 (1997) 1623–1629.
[80] H. Nakayama, N. Wada, M. Tsuhako, Int. J. Pharm. 269 (2004) 469–478.
[81] P.K. Dutta, D.S. Robins, Langmuir 10 (1994) 1851–1856.
[82] H. Yan, J. Lu, M. Wei, J. Ma, H. Li, J. He, D.G. Evans, X. Duan, J. Mol. Struct. Theochem. 866 (2008) 34–45.
[83] P. Baranek, A. Lichanot, R. Orlando, R. Dovesi, Chem. Phys. Lett. 340 (2001) 362–369.
[84] S.T. Zhang, H. Yan, M. Wei, D.G. Evans, X. Duan, J. Phys. Chem. C 116 (2012) 3421–3431.
[85] H.C. Andersen, J. Chem. Phys. 72 (1980) 2384–2393.
[86] H.J.C. Berendsen, J.P.M. Postma, W.F. van Gunsteren, A. DiNola, J.R. Haak, J. Chem. Phys. 81 (1984) 3684–3690.
[87] Discover, User Guide, Accelrys, Molecular Simulations Inc., San Diego, USA, 1996.
[88] E.Y. Tyunina, V.G. Badelin, G.N. Tarasova, Russ. J. Phys. Chem. A 89 (2015) 1595–1598.
[89] A.W. Herlinger, T.N. Long, J. Am. Chem. Soc. 92 (1970) 6481–6486.
[90] S. Venyaminov, N.N. Kalnin, Biopolymers 30 (1990) 1243–1257.
[91] T.F. Pauwels, W. Lippens, P.W. Smet, G.G. Herman, A.M. Goeminne, Polyhedron 18 (1999) 1029–1037.
[92] A. Barth, Prog. Biophys. Mol. Biol. 74 (2000) 141–173.
[93] A.R. Garcia, R.B. de Barros, J.P. Lourenço, L.M. Ilharco, J. Phys. Chem. A 112 (2008) 8280–8287.
[94] J. Oomens, J.D. Steill, B. Redlich, J. Am. Chem. Soc. 131 (2009) 4310–4319.
[95] M. Wolpert, P. Hellwig, Spectrochim. Acta Part A 64 (2006) 987–1001.
[96] V. Prevot, C. Forano, J.P. Besse, Inorg. Chem. 37 (1998) 4293–4301.
[97] M. Kakihana, T. Nagumo, J. Phys. Chem. 91 (1987) 6128–6136.
[98] W. Zhuang, M. Marigo, K.A. Jørgensen, Org. Biomol. Chem. 3 (2005) 3883–3885.
[99] L. Huang, X. Yao, Y. An, C. Peng, Adv. Mater. Res. 512–515 (2012) 2361–2365.
[100] D. Enders, T.V. Nguyen, Tetrahedron Lett. 53 (2012) 2091–2095.
[101] Z. Yang, H. Zeng, X. Zhou, H. Ji, Tetrahedron 68 (2012) 5912–5919.
[102] H. Chen, H. Ji, X. Zhou, L. Wang, Tetrahedron 66 (2010) 9888–9893.
[103] B. Capon, Z.P. Wu, J. Org. Chem. 55 (1990) 2317–2324.
[104] D.R. Boyd, W.B. Jennings, L.C. Waring, J. Org. Chem. 51 (1986) 992–995.
[105] R.A. Clark, D.C. Parker, J. Am. Chem. Soc. 93 (1971) 7257–7261.
[106] H. Liu, Z. An, J. He, ACS Catal. 4 (2014) 3543–3550.
[107] J. Wang, L. Zhao, H. Shi, J. He, Angew. Chem. Int. Ed. 50 (2011) 9171–9176.
[108] L. Zhao, H. Shi, J. Wang, J. He, J. Chem. Eur. 18 (2012) 15323–15329.
[109] K. Kalyanasundaram, J.K. Thomas, J. Am. Chem. Soc. 99 (1977) 2039–2044.
[110] A. Hillgren, H. Evertsson, M. Alden, Pharm. Res. 19 (2002) 504–510.
[111] L. Mohanambe, S. Vasudevan, Langmuir 21 (2005) 10735–10742.
[112] L. Mohanambe, S. Vasudevan, J. Phys. Chem. B 110 (2006) 14345–14354.
[113] N. Ménard, N. Tsapis, C. Poirier, T. Arnauld, L. Moine, F. Lefoulon, J.M. Péan, E. Fattal, Eur. J. Pharm. Sci. 44 (2011) 595–601.
[114] S.J. Chen, B. Chen, H.Q. Zhu, C.S. Wang, X.Y. Wu, P. Lv, Pet. Sci. 14 (2017) 195–202.
[115] M. Koyanagi, J. Mol. Spectrosc. 25 (1968) 273–290.
[116] G.W. Robinson, J. Chem. Phys. 46 (1967) 572–585.